K-Band Electromagnetic Wave Absorption of Ni-Co-Substituted Ba-W Hexaferrites Prepared via Sol-Gel Method with Molten Salt

Min Jang^{1,2†}, Horim Lee^{2†}, Je In Lee^{1*}, and Byeongjin Park^{2*}

¹School of Materials Science and Engineering, Pusan National University, 2 Busandaehak-ro 63beon-gil, Geumjeong-gu, Busan 46241, Republic of Korea

(Received 13 June 2025, Received in final form 26 June 2025, Accepted 26 June 2025)

The demand for thin and broadband high-frequency electromagnetic wave absorbers has grown rapidly with the advancement of communication technologies. However, most conventional magnetic materials exhibit ferromagnetic resonance (FMR) at low frequencies, restricting their applicability in high-frequency ranges such as the K-band, which is widely used in 5G communication. In this study, Ni-Co-substituted Ba-W hexaferrites (BaNi_{2-x}Co_xFe₁₆O₂₇) were synthesized via a citric acid-assisted sol–gel method combined with molten salt calcination to achieve single-phase formation at a reduced temperature of 1250 °C. By adjusting the Ni and Co substitution levels, the FMR frequency was effectively tuned within the 18–40 GHz range. The composite absorber with the optimized composition, BaNi_{1.4}Co_{0.6}Fe₁₆O₂₇, exhibited over 90% absorption efficiency across the entire K-band with a minimal thickness of 1.2 mm. This absorber outperforms many previously reported materials by offering wider bandwidth and thinner thickness. These findings highlight the suitability of Ni-Co-substituted Ba-W hexaferrites for next-generation communications.

Keywords: W-type hexaferrite, Ferromagnetic resonance, Electromagnetic wave absorber, Reflection loss

1. Introduction

Advancements in modern electronics and communication technologies have led to a growing shift toward higher-frequency operation beyond traditional sub-3 GHz bands. Frequencies above 10 GHz offer advantages such as increased data transmission speeds, enhanced reliability, and higher network capacity. For instance, 5G communications utilize millimeter-wave (mmWave, 30–300 GHz) bands to enable ultra-fast mobile internet, real-time data transfer, and vehicle-to-vehicle connectivity. In addition, the K-band (18–26.5 GHz) is widely used in automotive radar, satellite communications, and military tracking systems, and is emerging as a key candidate for future 6G systems due to its broader coverage and lower propagation loss compared to higher mmWave frequencies.

However, the rapid expansion of these frequency bands has raised concerns regarding electromagnetic interference (EMI), thereby increasing the demand for thin, broadband electromagnetic wave absorbers [1, 2]. Achieving efficient absorption in this context requires materials that possess high complex permittivity and permeability. While higher values of these parameters shorten the effective wavelength ($\lambda = c/\sqrt{\mu_r \varepsilon_r}$), where c is the speed of light in vacuum), an excessive increase in permittivity can lead to impedance mismatch with free space (where $\varepsilon_r = \mu_r = 1$), causing greater surface reflection and reduced absorption [3].

Magnetic materials are therefore of interest, as their high permeability enables improved impedance matching [4]. In particular, ferromagnetic resonance (FMR) plays a critical role in enhancing permeability above microwave frequencies [5]. Nevertheless, most conventional magnetic materials such as Fe, Co, and spinel ferrites exhibit FMR below a few GHz, limiting their utility in high-frequency applications.

Among various magnetic candidates, hexagonal ferrites especially W-type hexaferrites have gained attention due to their intrinsically high FMR frequencies (~40 GHz), strong magnetocrystalline anisotropy, and elevated permeability [6, 7]. Structurally, W-type hexaferrites adopt an

©The Korean Magnetics Society. All rights reserved.

*Corresponding author: Tel: +82-55-280-3161

Fax: +82-55-280-3269, e-mail: jilee@pnu.ac.kr, b.park@kims.re.kr

[†]These authors contributed equally to this work.

²Korea Institute of Materials Science, 797 Changwonadero, Seongsan-gu, Changwon, Gyeongnam 51508, Republic of Korea

M+2S configuration, combining one M-type block with two spinel blocks arranged in a specific stacking order (RSSR.SS*) [8]. Despite these advantages, several obstacles hinder their practical use. The synthesis of single-phase W-type hexaferrites typically requires high calcination temperatures exceeding 1495 °C [9, 10], and few studies have reported successful low-temperature synthesis processes [11, 12]. Additionally, tuning the FMR frequency of W-type hexaferrites to match specific absorption bands remains a challenge, and only limited research has demonstrated FMR shifts into technologically relevant bands like the K-band [13-15].

In this study, we address these challenges by synthesizing Ni-Co-substituted Ba-W hexaferrites (BaNi_{2-x}Co_x-Fe₁₆O₂₇) via a citric acid-assisted sol-gel method combined with molten salt calcination. The key contributions of this work are threefold: (1) We successfully synthesized single-phase Ni-Co-substituted Ba-W hexaferrite at a significantly reduced calcination temperature of 1250 °C. (2) The FMR frequency of the Ba-W ferrite was effectively tuned within the 18-40 GHz range by adjusting the Ni and Co content. (3) A composite absorber based on BaNi_{1.4}Co_{0.6}Fe₁₆O₂₇ demonstrated broadband absorption across the entire K-band (18.14–26.5 GHz) at a remarkably thin thickness of just 1.2 mm. These findings demonstrate the strong potential of Ni-Cosubstituted Ba-W hexaferrites for high-frequency applications such as EMI shielding and wave absorption in next-generation communication systems.

2. Experimental

2.1. Materials

The raw materials used in this study included barium nitrate (Ba(NO₃)₂, Sigma–Aldrich, ≥99%), iron nitrate nonahydrate (Fe(NO₃)₃·9H₂O, Duksan, Korea), nickel nitrate hexahydrate (Ni(NO₃)₂·6H₂O, Sigma–Aldrich), cobalt(II) nitrate hexahydrate (Co(NO₃)₂·6H₂O, Sigma

–Aldrich, ≥98%), sodium chloride (NaCl, Duksan, Korea), and citric acid monohydrate (C₆H₈O₇·H₂O, Samchun, Korea). A thermoplastic polyurethane (TPU) binder solution, consisting of 30 wt% TPU dissolved in a solvent mixture of N,N-dimethylformamide (DMF) and methyl ethyl ketone (MEK) was supplied by Songwon Industrial (Korea) and used as the polymer matrix for the absorber preparation.

2.2. Preparation of W-type hexaferrite powder

Ni-Co-substituted Ba-W hexaferrite powder was synthesized using a citric acid-assisted sol-gel method [16]. followed by high-temperature calcination in the presence of molten salt [17]. Stoichiometric quantities of barium nitrate, iron (III) nitrate nonahydrate, nickel (II) nitrate hexahydrate, cobalt (II) nitrate hexahydrate, and citric acid monohydrate were dissolved in deionized water to form the precursor solution. This solution was heated at 90 °C for 24 hours to evaporate the water, yielding a dried gel. The resulting solid was ground into fine powder and calcined at 1250 °C for 3 hours in the presence of 50 wt% NaCl. After calcination, residual NaCl was removed by washing with deionized water. The final product was dried at 130 °C for 24 hours in a convection oven.

2.3. Preparation of the electromagnetic wave absorber composites

The electromagnetic absorber composites were fabricated by mixing the Ni-Co-substituted Ba-W hexaferrite powder with the TPU solution at a weight ratio of 70:30. The mixture was homogenized using a planetary paste mixer (ARE-310, THINKY, Japan) at 2000 rpm for 3 minutes, followed by a defoaming step at 2200 rpm for 2 minutes. The resulting paste was dried at 130 °C for 24 hours and then compression-molded at 150 °C using a high-temperature hydraulic press to produce absorber films of the desired thickness. The fabricated composite

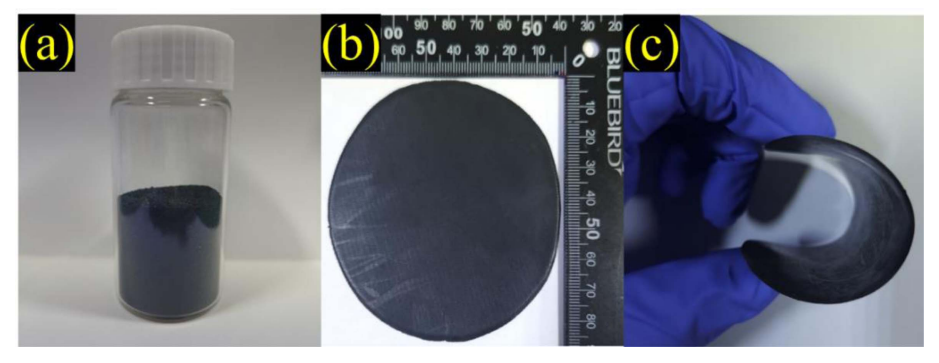


Fig. 1. (Color online) (a) W-type hexaferrite powder (b) W-type hexaferrite film (c) Flexibility of the W-type hexaferrite film.

absorber film is shown in Fig. 1(b) and (c).

2.4. Characterization

The morphology of the Ni-Co-substituted Ba-W hexaferrite powders was examined using scanning electron microscopy (SEM, JSM-7001F, JEOL). Phase identification and crystallographic analysis were carried out by X-ray diffraction (XRD, D/MAX 2500, RIGAKU) using Cu Kα radiation. Magnetic hysteresis loops were obtained using a vibrating sample magnetometer (EZ9 VSM, MicroSense) under an applied magnetic field of ±25 KOe. The complex permittivity and permeability of the composites were measured using a vector network analyzer (N5291A, Keysight) in conjunction with a waveguide (K11644A, Keysight) and free-space measurement system (FS-110, EMLabs) across two different frequency bands: K-band (18-26.5 GHz) and Ka-band (26.5-40 GHz). Waveguide-based measurements were employed for the K-band, while the Ka-band measurements were conducted using a free-space system.

3. Results and Discussion

3.1. Microstructure of Ni-Co-substituted Ba-W hexaferrites

Fig. 2 displays scanning electron microscopy (SEM) images of BaNi_{2-x}Co_xFe₁₆O₂₇ powders, representing Ni-

Co-substituted Ba-W hexaferrites with Co substitution levels ranging from x = 0 to 0.6. All samples were subjected to calcination in the presence of molten NaCl, which promoted particle growth and crystallization by enhancing Ba²⁺ ion transport within the NaCl liquid phase. Across the entire Ni-Co substitution range, hexagonal plate-like particles with an average diameter of ~15 μm and thickness of ~2 μm were consistently formed. Notably, no significant changes in particle morphology—such as size, shape, or aspect ratio—were detected with increasing Co content, indicating that Co ion substitution does not substantially alter the particle morphology of W-type hexaferrites.

Fig. 3 presents the X-ray diffraction (XRD) patterns of BaNi_{12-x}Co_xFe₁₆O₂₇ powders with varying Co substitution levels(x) from 0 to 0.6. All samples exhibited diffraction peaks that aligned well with the characteristic reflections of the single-phase W-type hexaferrite structure [18]. Unlike M-type or X-type hexaferrites, W-type hexaferrites are typically stable only at temperatures exceeding 1400 °C. Remarkably, in this study, single-phase Ni-Co-substituted Ba-W hexaferrites were successfully synthesized at a relatively low calcination temperature of 1250 °C through the molten salt method. This result can be attributed to the role of molten NaCl, which enhances mass transport in the liquid phase due to its high solubility for Ba²⁺ ions a mechanism previously reported

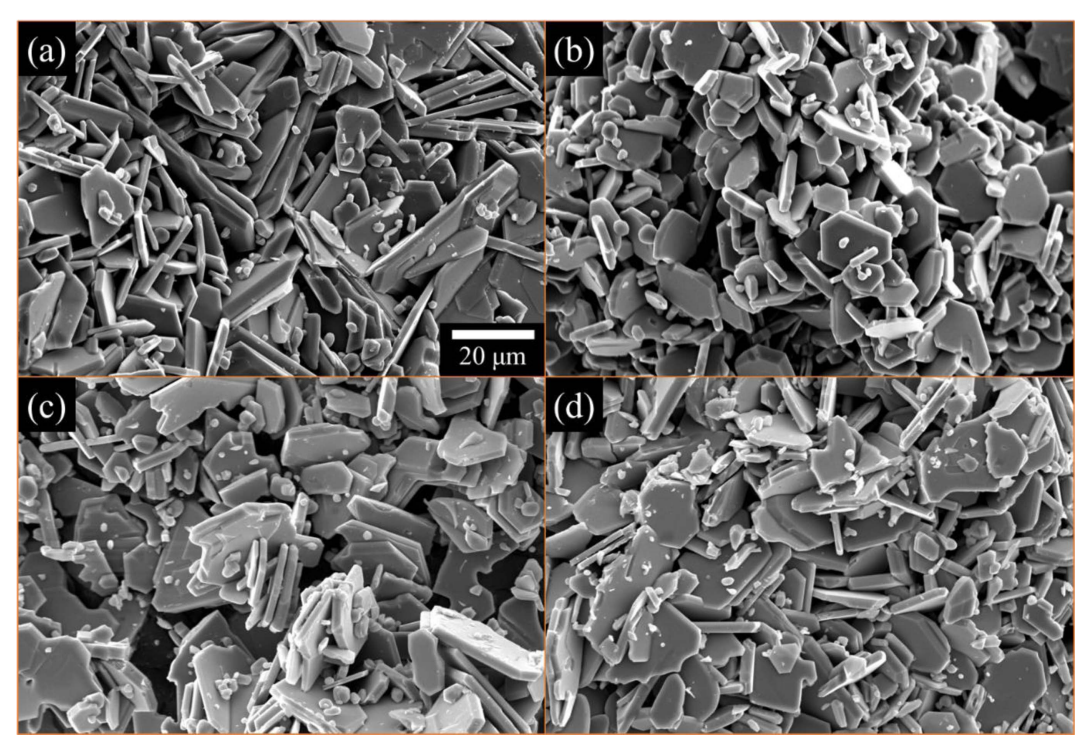


Fig. 2. SEM image of BaNi_{2-x}Co_xFe₁₆O₂₇: (a) x=0, (b) x=0.2, (c) x=0.4, (d) x=0.6.

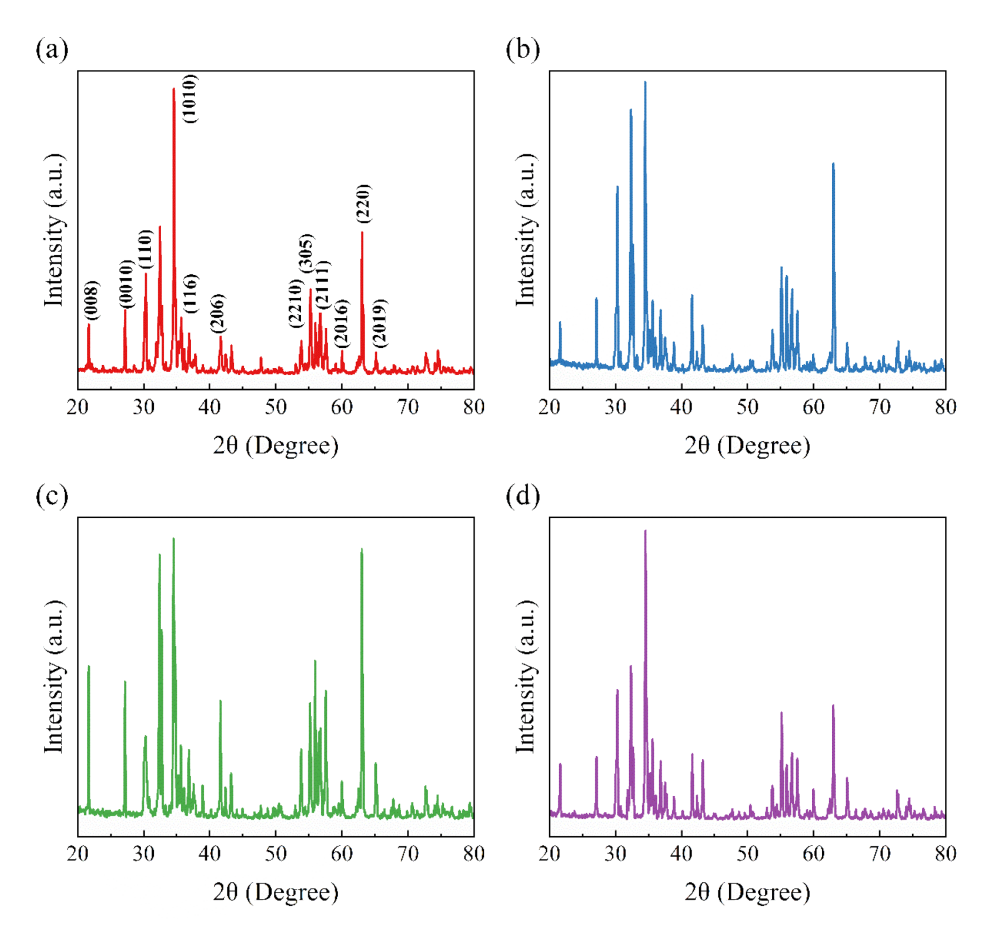


Fig. 3. (Color online) XRD pattern of BaNi_{2-x}Co_xFe₁₆O₂₇: (a) x=0, (b) x=0.2, (c) x=0.4, (d) x=0.6.

to assist in forming single-phase W-type hexaferrites [19]. In the molten state, NaCl acts as a reaction medium that promotes the dissolution of intermediate phases and enhances the diffusion of Ba²⁺ and Fe³⁺ ions, thereby accelerating the formation of the desired phase. This process follows a dissolution–precipitation mechanism, as previously observed in BaM systems [20], which enables more complete reactions at lower temperatures and suppresses the formation of secondary phases. Consequently, the molten salt-assisted sol-gel synthesis not only

Table 1. Calculated lattice constants of Ba-W hexaferrites with different composition.

Composition		Lattice constants			
		a (Å)	c (Å)	Volume (ų)	
(x=0)	$BaNi_{2.0}Fe_{16}O_{27}$	5.88	32.7	981.6	
(x=0.2)	$BaNi_{1.8}Co_{0.2}Fe_{16}O_{27}$	5.90	32.8	987.5	
(x=0.4)	$BaNi_{1.6}Co_{0.4}Fe_{16}O_{27} \\$	5.90	32.8	988.5	
(x=0.6)	BaNi _{1.4} Co _{0.6} Fe ₁₆ O ₂₇	5.90	32.8	990.4	

lowers the calcination temperature but also improves phase purity. In the present work, this effect is confirmed by the formation of well-defined, hexagonal plate-like particles with a pure W-type crystal structure.

The lattice parameters were determined from the XRD diffraction data, with the calculated values summarized in Table 1. For the sample with only Ni substitution, the lattice constants along the a- and c-axes were found to be 5.88 Å and 32.7 Å, respectively, which are consistent with previously reported values [21]. With increasing Co substitution, slight expansions were observed in both lattice constants and overall unit cell volume. This expansion is primarily attributed to the difference in ionic radii among the substituting ions. Specifically, the ionic radius of Co²⁺ (0.74 Å) is larger than those of Ni²⁺ (0.69 Å) and Fe³⁺ (0.64 Å); thus, the incorporation of Co²⁺ into the W-type hexaferrite lattice induces a gradual lattice expansion, reflected in the increased lattice parameters. Moreover, this lattice expansion further confirms the effective incorporation of Co²⁺ ions into the W-type hexaferrite crystal lattice.

3.2. Magnetic properties of Ni-Co-substituted W-type hexaferrites

The magnetic hysteresis loops of the Ni-Co-substituted Ba-W hexaferrite powders are shown in Fig. 4(a). Regardless of the Co substitution level, all samples exhibited soft magnetic behavior. Notably, all compositions achieved saturation magnetization (M_S) values exceeding 60 emu/g, suggesting high phase purity of the synthesized powders. The M_S of Ba-W hexaferrites arises from the combined magnetic contributions of ions located at seven distinct crystallographic sites within the unit cell: 4f₂, 6g, 4f₃, 4e, 4f₁, 12k, and 2d. Among these, the 12k, 4f₂, 6g, and 4f₃ sites are octahedral, the 4e and 4f₁ sites are tetrahedral, and the 2d site is bipyramidal [22]. Spin alignment at these sites varies: 6g, 4f₃, 12k, and 2d are spin-up, whereas 4f₂, 4e, and 4f₁ are spin-down. Therefore, the net M_S is determined by the vector sum of the magnetic moments from these seven sublattices with opposing spin directions. The magnetic moments of Co²⁺ and Ni²⁺ ions are 3 μB and 2 μB, respectively, which are smaller than that of Fe^{3+} (5 μB). Accordingly, substitution of Co^{2+} ions into spin-up Fe^{3+} sites is expected to lower the M_S , whereas substitution into spin-down sites should lead to an increase. However, as depicted in Fig. 4(b), the M_S values do not exhibit a clear trend with increasing Co content [23]. This inconsistency may be due to the Co^{2+} ions occupying both spin-up and spin-down sites, thereby mitigating their overall effect on the saturation magnetization.

As illustrated in Fig. 4(c), the H_C of Ni-Co-substituted Ba-W hexaferrites followed a different trend from that of the M_S . The highest H_C value of 424.1 Oe was observed for the sample containing only Ni substitution, while H_C steadily declined with increasing Co content, reaching a minimum of 92.8 Oe at x = 0.6. Coercivity in magnetic materials is governed by both extrinsic factors, such as particle size and morphology, and intrinsic properties, such as magnetocrystalline anisotropy. From the extrinsic perspective, H_C typically peaks when particle size approaches the critical single-domain size, and decreases when

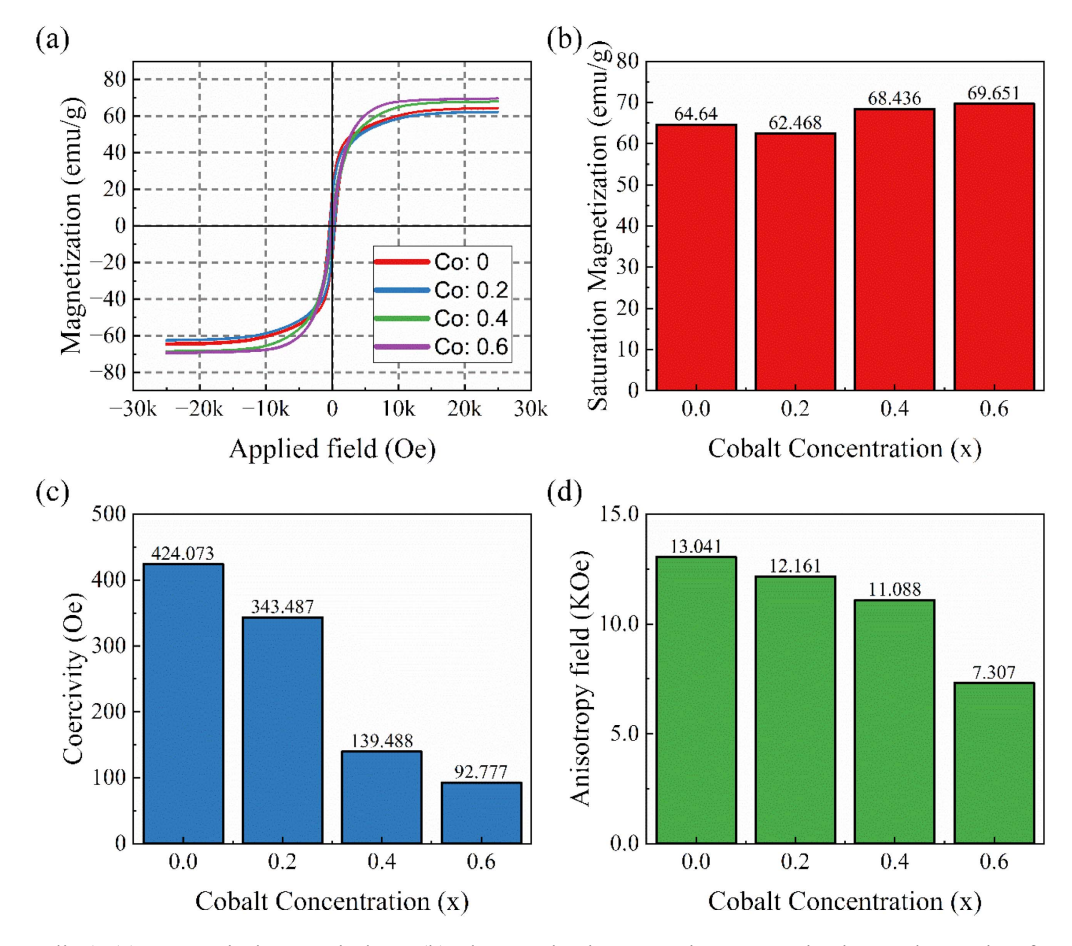


Fig. 4. (Color online) (a) Magnetic hysteresis loop (b) changes in the saturation magnetization and coercive force according to changes in the cobalt concentration.

Table 2. Summary of changes in M_S , H_C , and H_A with varying cobalt concentration.

Composition	Ms (emu/g)	Hc (Oe)	Ha (kOe)
$BaNi_{2.0}Fe_{16}O_{27}$	64.6	424.1	13.0
$BaNi_{1.8}Co_{0.2}Fe_{16}O_{27}$	62.5	343.5	12.2
$BaNi_{1.6}Co_{0.4}Fe_{16}O_{27}$	68.4	139.5	11.1
BaNi _{1.4} Co _{0.6} Fe ₁₆ O ₂₇	69.7	92.8	7.3

the size deviates from this optimum. Previous reports estimate this critical domain size for W-type hexaferrites to be approximately $2\,\mu m$ [24]. As shown in Fig. 2, the particle size of the Ni-substituted Ba-W hexaferrite exceeds this threshold, which explains its soft magnetic nature [25]. However, because Co substitution causes negligible changes in particle size, this factor alone cannot account for the pronounced reduction in H_C with increasing Co content. Instead, this trend is more

plausibly attributed to a reduction in magnetic anisotropy induced by Co incorporation. Specifically, Co substitution is known to lower magnetic anisotropy in hexaferrites by reorienting the easy axis of magnetization from the c-axis to the basal plane [26]. The anisotropy field (H_A) of all samples was calculated using the Law of Approach to Saturation (LAS) method. As shown in Fig. 4(d), H_A decreased with increasing Co substitution. This clearly indicates that the incorporation of Co ions leads to a reduction in magnetic anisotropy, which in turn provides a plausible explanation for the observed decrease in coercivity.

3.3. Electromagnetic properties of Ni-Co-substituted W-type hexaferrites

To assess the suitability of the synthesized Ba-W hexaferrites as high-frequency electromagnetic wave absorbers, Ba-W ferrite composite samples were fabricated according to the procedure described in Section 2.3.

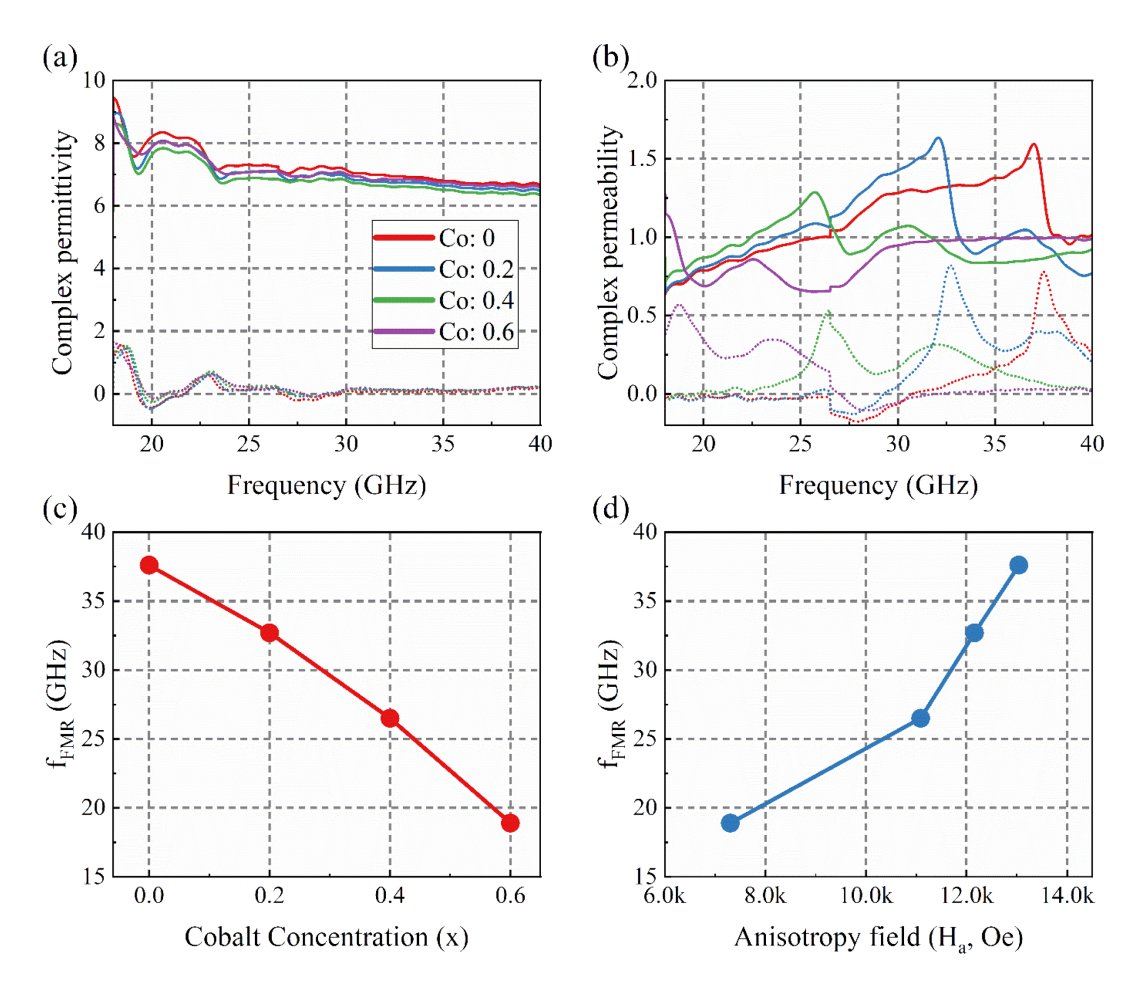


Fig. 5. (Color online) (a) Complex permittivity change due to the frequency change of $BaNi_{2-x}Co_xFe_{16}O_{27}$ (x=0, 0.2, 0.4, 0.6) (b) Complex permeability (c) Changes in the FMR frequency with changes in the cobalt concentration (d) Changes in the with FMR frequency changes in the anisotropy field (H_a).

Fig. 5(a) and (b) show the measured complex permittivity and permeability of Ba-W hexaferrite composites, with solid lines and dashed lines representing the real and imaginary parts, respectively. The permittivity remains nearly constant regardless of the Co substitution level, and all samples exhibit low dielectric loss, as shown in Fig. 5(a). These dielectric properties are consistent with previously reported results [6]. In contrast, Fig. 5(b) reveals distinct peaks in both the real and imaginary parts of the permeability, indicating the presence of notable magnetic loss. It should be noted that minor discontinuities in the measured data appear near the frequency band boundaries, at 26.5 GHz between the K-band and Ka-band, due to changes in the measurement system across different frequency ranges.

Importantly, the position of the resonance peak, which is corresponding to the ferromagnetic resonance (FMR) frequency, shifts toward lower frequencies as the Co substitution level increases, as shown in Fig. 5(c). This trend is consistent with the well-known relationship that the FMR frequency is proportional to the magnetic anisotropy field [27].

$$\int_{FMR} = \frac{\gamma}{2\pi} H_a = 1.4gH_a \tag{1}$$

where γ represents the gyromagnetic ratio and g is the Lande g-factor. As Co substitution increases, the anisotropy field of the Ni-Co-substituted Ba-W hexaferrite decreases due to a reduction in overall magnetocrystalline anisotropy caused by the incorporation of Co ions in Ba-W hexaferrite. This behavior is further supported by Fig. 5(d), which shows a clear linear relationship between magnetic anisotropy and FMR

frequency, as predicted by the above equation (1).

The electromagnetic wave absorption characteristics of the fabricated composite were evaluated by calculating the reflection loss (RL) using impedance matching theory [28]. The input impedance (Z_{in}) of the absorber was determined by the following equation:

$$Z_{in} = Z_0 \sqrt{\frac{\mu_r}{\varepsilon_r}} \tanh\left(\frac{2j\pi f d}{c} \sqrt{\mu_r \varepsilon_r}\right)$$
 (2)

where Z₀ is the electromagnetic characteristic impedance of free space, μ_r and ε_r represent complex permeability and permittivity, respectively. f is the frequency of the incident electromagnetic wave, d is the thickness of the absorber; and c is the speed of light in vacuum. When an electromagnetic wave propagates from free space toward an absorber, reflection may occur at the interface due to impedance mismatch between the two media. To minimize this reflection, impedance matching is crucial so that the incident wave can be effectively transmitted into the absorber. Once inside the material, the wave undergoes both phase alteration and amplitude attenuation, during which its electromagnetic energy is progressively converted into heat and dissipated. These energy loss processes are governed by the material's complex permittivity and permeability, giving rise from dielectric and/or magnetic losses. Consequently, achieving nearperfect absorption with minimal surface reflection requires precise tuning of the absorber's thickness, as well as its dielectric and magnetic properties.

Fig. 6(a) shows the calculated RL curves in the frequency range of K-band for various absorber thicknesses at a fixed composition of BaNi_{1.6}Co_{0.6}Fe₁₆O₂₇, exhibiting strong magnetic loss due to FMR in the K-band. For

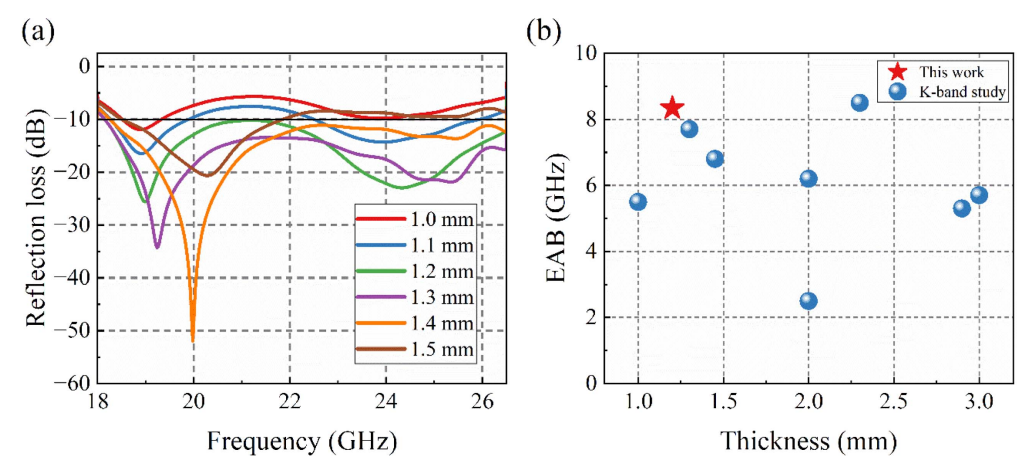


Fig. 6. (Color online) (a) Calculated RL values according to the thickness of the composite with the composition of BaNi_{1.4}Co_{0.6}Fe₁₆O₂₇ (b) Comparison of the performance of this study (Red Star) with previous K-band target absorber studies.

Table 3. Summary of maximum EAB and minimum RL values by thickness.

Thickness	Maximum EAB	Min RL	
(mm)	(GHz)	(dB)	
1.0	0.8	-11.9	
1.1	3.42	-14.3	
1.2	8.34	-25.	
1.3	8.34	-34.3	
1.4	8.24	-52.0	
1.5	3.32	-20.6	

practical electromagnetic wave absorption, an RL value below -10 dB is generally considered to be effective, corresponding to more than 90% absorption and defined as the effective absorption bandwidth (EAB). The optimal thickness was determined using the impedance matching model described in Equation (2), and this analysis revealed that a 1.2 mm-thick absorber achieved a broad EAB of 8.34 GHz, which is sufficient to cover the entire K-band. The corresponding EAB values and minimum RL for each thickness are summarized in Table 3. It can be found that with a thickness thinner or thicker than the optimized 1.2 mm, the EAB dramatically decreases. As the input impedance is dependent to the absorber thickness (Equation (2)), absorber thickness design is very important for the optimized absorber performance. In general, the optimized thickness is about a quarter of electromagnetic wavelength in the absorber.

and Table 4 compares the EAB and thickness of the present composite with those of previously reported K-band absorbers [29-36]. In general, a broader EAB achieved with reduced thickness indicates superior absorption performance. The comparison clearly demonstrates that the Ba-W hexaferrite absorber developed in

this study surpasses many previously reported absorbers, exhibiting outstanding application potential due to its wide absorption bandwidth even at a relatively thin thickness.

4. Conclusion

In this study, we developed a high-performance K-band electromagnetic wave absorber using Ni-Co-substituted Ba-W hexaferrite synthesized via a citric acid-assisted sol-gel method combined with molten salt calcination. This approach enabled the formation of a single-phase Wtype structure at a reduced temperature of 1250 °C. By adjusting the Ni and Co content, the FMR frequency was effectively tuned across the 18-40 GHz range, ensuring applicability to various high-frequency bands. Among the compositions, BaNi_{1.4}Co_{0.6}Fe₁₆O₂₇ exhibited excellent absorption performance, achieving over 90% absorption (RL < -10 dB) across the entire K-band (18.14-26.5 GHz)with a thickness of only 1.2 mm. This result outperforms many previously reported absorbers by offering wider bandwidth and thinner thickness. Overall, the findings highlight the strong potential of Ni-Co-substituted Ba-W hexaferrites as efficient materials for thin, broadband electromagnetic absorbers in advanced millimeter-wave applications, including 5G/6G communications, automotive radar, and EMI shielding.

Acknowledgements

This research was supported by the Fundamental Research Program of the Korea Institute of Materials Science (PNK9930) and the Technology Innovation Program (200250804) funded by the Ministry of Trade, Industry & Energy (MOTIE, Korea).

Table 4. Comparison of the performance of this study (Red Star) with previous K-band target absorber studies.

Material	Frequency Band (GHz)	Thickness (mm)	EAB (GHz)	RLmin (dB)	Ref
BaFe _{10.4} Nb _{0.8} Ni _{0.8} O ₁₉	18-24.8	1.45	6.8	-31.8	[29]
MoS2@HCS	21-25	1	5.5	-48	[30]
MWCNT@F _e 3O ₄	20.8-26.5	3	5.7	-32.3	[31]
Fe ₃ O ₄ @CNT@CF	21.2-26.5	2.9	5.3	-49.46	[32]
$BaFe_{10}CO_{1.0}Ti_{1.0}O_{19}$	18-24.2	2	6.2	-22.7	[33]
CNT@CNFs	18.4-26.4	1.3	7.7	-43	[34]
$Ni_{0.6}Zn_{0.4}(CoZr)_{0.25}Fe_{1.5}O_4$	18-20.5	2	2.5	-26	[35]
$ZnFe_2O_4$	18-26.5	2.3	8.5	-40.33	[36]
$BaNi_{1.4}Co_{0.6}Fe_{16}O_{27}$	18.14-26.5	1.2	8.34	-34.3	This work

References

- R. K. Mishra, R. D. Gupta, and S. Datar, Plasmonics 16, 2061 (2021).
- [2] D. Micheli, R. Pastore, C. Apollo, M. Marchetti, G. Gradoni, V. M. Primiani, and F. Moglie, IEEE Transactions on Microwave Theory and Techniques 59, 2633 (2011).
- [3] M. A. Butt and N. L. Kazansky, Photonics Letters of Poland 12, 88 (2020).
- [4] D. C. Jiles and D. L. Atherton, J. Magn. Magn. Mater. 61, 48 (1986).
- [5] V. Sharma, J. Saha, S. Patnaik, and B. K. Kuanr, J. Magn. Magn. Mater. 439, 277 (2017).
- [6] S.-M. Lee, T.-W. Lee, and Y.-M. Kang, J. Alloy Compd. 962, 171060 (2023).
- [7] H. Zhang, Z. Liu, X. Yao, L. Zhang, and M. Wu, J. Solgel Sci. Technol. 27, 277 (2003).
- [8] S. H. Mahmood, M. D. Zaqsaw, O. E. Mohsen, A. Awadallah, I. Bsoul, M. Awawdeh, and Q. I. Mohaidat, Solid State Phenomena 241, 93 (2016).
- [9] N. Langhof, D. Seifert, M. Göbbels, and J. Töpfer, J. Solid State Chem. **182**, 2409 (2009).
- [10] C. Yu, A. S. Sokolov, P. Kulik, and V. G. Harris, J. Alloy Compd. 814, 152301 (2020).
- [11] M. M. Ali, O. M. Hemeda, and A. M. A. Henaish, J. Mater. Sci.: Mater. Electron. **32**, 16038 (2021).
- [12] L. Chang, X. Ren, H. Yin, Y. Tang, X. Pu, and H. Yuan, J. Mater. Sci.: Mater. Electron. 31, 20908 (2020).
- [13] J.-H. Heo and Y.-M. Kang, Appl. Sci. 14, 10631 (2024).
- [14] J.-U. Kim and Y.-M. Kang, Appl. Sci. 11, 8669 (2021).
- [15] K. A. Korolev, C. Wu, Z. Yu, K. Sun, M. N. Afsar, and V. G. Harris, AIP Adv. 8, 056440 (2018).
- [16] X. Wang, X. Chen, L. Gao, H. Zheng, M. Ji, T. Shen, and Z. Zhang, J. Cryst. Growth 256, 123 (2003).
- [17] S. Dursun, R. Topkaya, N. Akdoğan, and S. Alkoy, Ceram. Int. **38**, 3801 (2012).
- [18] S. H. Mahmood, Q. Al Sheyab, I. Bsoul, O. Mohsen, and A. Awadallah, Curr. Appl. Phys. **18**, 590 (2018).
- [19] Z. H. Yang, Z. W. Li, and Y. H. Yang, Mater. Chem.

- Phys. 144, 568 (2014).
- [20] H. Li, X. Yi, Y. Wu, X. Wei, D. Deng, L. Zheng, W. Luo, X. Luo, R. Gong, and M. Zhang, J. Alloys Compd. 827, 154083 (2020).
- [21] M. A. Iqbal, W. Tahir, G. Murtaza Rai, N. A. Noor, S. Ali, and K. T. Kubra, Ceram. Int. 38, 3757 (2012).
- [22] R. C. Pullar, Prog. Mater. Sci. 57, 1191 (2012).
- [23] J.-H. You, H.-J. Kim, and S.-I. Yoo, J. Alloy Compd. **695**, 3011 (2017).
- [24] Z. Su, Y. Chen, B. Hu, A. S. Sokolov, S. Bennett, L. Burns, X. Xing, and V. G. Harris, J. Appl. Phys. 113, 17B305 (2013).
- [25] G. Qi, Y. Liu, Y. Chen, Q. Liu, J. Chen, Q. Yin, and H. Zhang, J. Mater. Sci.: Mater. Electron. 32, 25769 (2021).
- [26] H. Graetsch, F. Haberey, R. Leckebusch, M. Rosenberg, and K. Sahl, IEEE Transa. Magn. 20, 495 (1984).
- [27] H. Lee, S. H. Ryu, S. J. Kwon, J. R. Choi, S.-b. Lee, and B. Park, Nanomicro. Lett. 15, 76 (2023).
- [28] S. J. Cheon, J. R. Choi, S.-b. Lee, J. I. Lee, and H. Lee, J. Alloys Compd. 976, 173019 (2024).
- [29] C. Liu, Y. Zhang, Y. Tang, Z. Wang, N. Ma, and P. Du, J. Mater. Chem. C 5, 3461 (2017).
- [30] M. Ning, Q. Man, G. Tan, Z. Lei, J. Li, and R. W. Li, ACS Appl. Mater. Interfaces 12, 20785 (2020).
- [31] C. Liu, Y. Xu. B. Huang, W. Zhang, and Y. Wang, Polymers 16, 2677 (2024).
- [32] L. Dewangan, M. S. Patinavalasa, J. Acharjee, Y. Solunke, S. Ghosh, and N. K. Mishra, AEU - Int. J. Electron. Commun. 170, 154828 (2023).
- [33] P. Kaur, P. Harshapriya, D. Basandrai, A. Arora, V. Kaur, A. Singh, and S. B. Narang, Mater. Sci. Eng.: B 313, 117888 (2025).
- [34] H. Dogari, H. Ghafuri, and R. Peymanfar, Adv. Sustain. Syst. 9, 2400793 (2025).
- [35] N. Aggarwal and S. B. Narang, Journal of Electronic Materials **50**, 5338 (2021).
- [36] Y. Ge, C. Li, G. I. N. Waterhouse, Z. Zhang, and L. Yu, Ceram. Int. **47**, 1728 (2021).